Mon. Not. R. Astron. Soc. **000**, 1–8 (1998) Printed 18 June 1998 (MN LaTeX style file v1.4)

Statistics of dark matter haloes expected from weak lensing surveys

Guido Kruse & Peter Schneider
Max-Planck-Institut für Astrophysik, Postfach 1523, D-85740, Garching, Germany

Accepted . Received ; in original form

ABSTRACT

The distortion of the images of faint high-redshift galaxies can be used to probe the intervening mass distribution. This weak gravitational lensing effect has been used recently to study the (projected) mass distribution of several clusters at intermediate and high redshifts. In addition, the weak lensing effect can be employed to detect (dark) matter concentrations in the Universe, based on their mass properties alone. Thus it is feasible to obtain a mass-selected sample of 'clusters', and thereby probe the full range of their mass-to-light ratios. We study the expected number density of such haloes which can be detected in ongoing and future deep wide-field imaging surveys, using the number density of haloes as predicted by the Press-Schechter theory, and modeling their mass profile by the 'universal' density profile found by Navarro, Frenk & White. We find that in all cosmological models considered, the number density of haloes with a signal-to-noise ratio larger than 5 exceeds 10 per square degree. With the planned MEGACAM imaging survey of ~ 25 deg^2, it will be easily possible to distinguish between the most commonly discussed cosmological parameter sets.

Key words: cosmology – gravitational lensing – clusters of galaxies – dark matter

1 INTRODUCTION

As first discussed by Webster (1985), the tidal gravitational field of clusters of galaxies distorts the images of background galaxies in a characteristic way. After the first extreme cases of distortions in the form of giant luminous arcs were discovered (Soucail et al. 1987; see Fort & Mellier 1994 for a review), much weaker coherent distortions of images were found (Fort et al. 1988; Tyson, Valdes & Wenk 1990). These distortions can be used to reconstruct the projected mass distribution of galaxy clusters in a non-parametric way (Kaiser & Squires 1993).

In addition, as pointed out in Schneider (1996; hereafter S96), the search for coherent image alignments can be used to search for (dark) mass concentrations. Generalizing the aperture densitometry of Kaiser (1995; see also Kaiser et al. 1994), it was shown in S96 that haloes with characteristic velocity dispersions of ≥ 600 km/s can be significantly detected on deep high-quality optical images, such as can be obtained with a 4-metre class telescope at the best sites. Indeed, there are first reports of detections of mass concentrations selected by this weak lensing technique (Luppino & Kaiser 1997; T. Erben, private communication) which coincide with a concentration of galaxies; they are most likely genuine clusters. Seitz et al. (1998) have provided a thorough lensing analysis of the cluster MS1512+36 which acts as a strong gravitational telescope on the $z = 2.72$ galaxy cB58 detected by Yee et al. (1996). Whereas this cluster appears to have a velocity dispersion of order 600 km/s, it nevertheless shows up with very high significance in the weak lensing analysis, using only 33 (background) galaxies and excluding the strong lensing features, thus observationally verifying the estimate of S96.

The detection of mass concentrations by weak lensing techniques therefore offers the opportunity to define a mass-selected sample of haloes. In contrast to the usual selection procedures, based on emitted light (in the optical or X-ray waveband), the resulting sample would be 'mass-limited', rather than of flux limited. Such a sample would therefore be extremely useful for cosmological purposes, since it can directly be compared to theoretical predictions, e.g., derived from N-body simulations. In contrast, the comparison of optically-selected cluster samples with cosmological predictions involves assumptions about the relation between mass and light, and the mass-to-light ratio may vary strongly between individual clusters. Given that the evolution of clusters with redshift is among the strongest tests for distinguishing between different cosmogonies (see, e.g., White, Efstathiou & Frenk 1993; Eke, Cole & Frenk 1996; Bartelmann et al. 1998; Borgani et al. 1998, and references therein), their mass-based detection would indeed be of great interest. A mass-selected sample of haloes may lead to the detection of clusters with very faint emission which could be missed by other selection criteria.

The basic method discussed in S96 is to use the aperture mass $M_{\rm ap}(\theta)$ technique (Kaiser 1995; Squires & Kaiser 1996) on deep wide-field images. The aperture mass is the projected density field of the mass inhomogeneities between us and the population of faint high-redshift galaxies, weighted by a redshift-dependent term and filtered through a function of zero net weight (e.g., a Mexican hat). The advantage of this measure is that it can be expressed directly in terms of the shear, for which the observed image ellipticities provide an unbiased estimate. Thus, an estimate for the aperture mass can be expressed directly in terms of observables, with well defined signal-to-noise ratio. Hence, a (dark) matter concentration would be 'seen' as a high S/N peak in the aperture mass map.

In this paper, we investigate the statistics of such peaks in various cosmological models. The number density of haloes is calculated using the Press-Schechter (1974) formalism, and their density profile is approximated by the universal halo profile found by Navarro, Frenk & White (1996, 1997; hereafter NFW). In Sect. 2 we summarize our method, and estimate signal-to-noise statistics in Sect. 3. The number of haloes of given $M_{\rm ap}(\theta)$, as a function of filter scale θ, and source and lens redshift, is derived in Sect. 4. We discuss the degree to which observations can be used to distinguish between these various cosmologies in Sect. 5, and present our conclusions in Sect. 6.

2 FORMALISM

Following S96, we define the spatially filtered mass inside a circular aperture of angular radius θ,

$$M_{\rm ap}(\theta) := \int d^2\vartheta\ \kappa(\boldsymbol{\vartheta})\ U(|\boldsymbol{\vartheta}|), \tag{1}$$

where the continuous weight function $U(\vartheta)$ vanishes for $\vartheta > \theta$. If $U(\vartheta)$ is a compensated filter function,

$$\int_0^\theta d\vartheta\ \vartheta\ U(\vartheta) = 0, \tag{2}$$

one can express $M_{\rm ap}$ in terms of the tangential shear inside the circle

$$M_{\rm ap}(\theta) = \int d^2\vartheta\ \gamma_{\rm t}(\boldsymbol{\vartheta})\ Q(|\boldsymbol{\vartheta}|), \tag{3}$$

where

$$\gamma_{\rm t}(\boldsymbol{\vartheta}) = -{\rm Re}(\gamma(\boldsymbol{\vartheta})e^{-2i\phi}) \tag{4}$$

is the tangential component of the shear at position $\boldsymbol{\vartheta} = (\vartheta\cos\phi, \vartheta\sin\phi)$, and the function Q is related to U by

$$Q(\vartheta) = \frac{2}{\vartheta^2}\int_0^\vartheta d\vartheta'\ \vartheta'\ U(\vartheta')\ - U(\vartheta). \tag{5}$$

We use a filter function from the familiy given in Schneider et al. (1998), specifically we choose the one with $l=1$. Then writing $U(\vartheta) = u(\vartheta/\theta)/\theta^2$, and $Q(\vartheta) = q(\vartheta/\theta)/\theta^2$,

$$u(x) = \frac{9}{\pi}(1-x^2)\left(\frac{1}{3}-x^2\right), \tag{6}$$

and

$$q(x) = \frac{6}{\pi}x^2(1-x^2), \tag{7}$$

with $u(x)=0$ and $q(x)=0$ for $x>1$. We will describe the mass density of dark matter haloes with the universal density profile introduced by NFW,

$$\rho(r) = \frac{3H_0^2}{8\pi G}\ (1+z)^3\ \frac{\Omega_{\rm d}}{\Omega(z)}\ \frac{\delta_c}{r/r_{\rm s}(1+r/r_{\rm s})^2}, \tag{8}$$

with

$$\Omega(z) = \frac{\Omega_{\rm d}}{a+\Omega_{\rm d}(1-a)+\Omega_{\rm v}(a^3-a)},\ a=\frac{1}{1+z}. \tag{9}$$

$\Omega_{\rm d}$ and $\Omega_{\rm v}$ denote the present day density parameters in dust and in vacuum energy respectively. Haloes identified at redshift z with mass M are described by the characteristic density contrast $\delta_{\rm c}$ and the scaling radius $r_{\rm s} = r_{200}/c$ where c is the concentration parameter (which is a function of $\delta_{\rm c}$), and r_{200} is the virial radius defined such that a sphere with radius r_{200} of mean interior density 200 $\rho_{\rm crit}$ contains the halo mass M_{200}. We compute the parameters which specify the NFW profile according to the description in NFW using the fitting formulae given there.

The surface mass density of the NFW-profile is given by (see Bartelmann 1996)

$$\Sigma(\vartheta) = \frac{3H_0^2}{4\pi G}\ (1+z)^3\ \frac{\Omega_{\rm d}}{\Omega(z)}\ r_{\rm s}\ \delta_{\rm c}\ f\left(\frac{\vartheta}{\theta_{\rm s}}\right) \tag{10}$$

with

$$f(x) = \frac{1}{x^2-1}\ \times \left\{ \begin{array}{ll} 1-\frac{2}{\sqrt{1-x^2}}\ {\rm arctanh}\sqrt{\frac{1-x}{1+x}}, & \text{for } x<1 \\ 1-\frac{2}{\sqrt{x^2-1}}\ {\rm arctan}\sqrt{\frac{x-1}{1+x}}, & \text{for } x>1 \end{array} \right., \tag{11}$$

and $\theta_{\rm s} = r_{\rm s}/D_{\rm d}$. $D_{\rm d}$ is the angular diameter distance to the lens. Introducing the critical surface density

$$\Sigma_{\rm cr} = \frac{c^2}{4\pi G}\ \frac{D_{\rm s}}{D_{\rm d}D_{\rm ds}} \tag{12}$$

with $D_{\rm s}$ and $D_{\rm ds}$ being the angular diameter distances to the source and from the lens to the source, we define the dimensionless surface mass density (convergence) which is a function of source redshift

$$\kappa(\vartheta, z_{\rm d}, z_{\rm s}) = \frac{\Sigma(\vartheta)}{\Sigma_{\rm cr}} = \kappa_0\ f\left(\frac{\vartheta}{\theta_{\rm s}}\right), \tag{13}$$

with

$$\kappa_0 = 3\ (1+z)^3\ \frac{\Omega_{\rm d}}{\Omega(z)}\ r_{\rm s}\ \frac{H_0^2}{c^2}\ \delta_c\ \frac{D_{\rm d}D_{\rm ds}}{D_{\rm s}}. \tag{14}$$

The second important quantity for lensing effects is the complex shear defined by

$$\gamma = \gamma_1 + i\gamma_2,\ \gamma_1 = \frac{1}{2}(\psi_{11}-\psi_{22}),\ \gamma_2 = \psi_{12}, \tag{15}$$

where ψ is given by the two-dimensional Poisson equation

$$\nabla^2\psi = 2\kappa. \tag{16}$$

In the case of an axi-symmetric density profile, the magnitude of the shear is given by

$$|\gamma(\vartheta)| = \left|\frac{m(\vartheta)}{\vartheta^2} - \kappa(\vartheta)\right|, \tag{17}$$

where

$$m(\vartheta) = 2\int_0^{\vartheta} d\vartheta' \; \vartheta' \kappa(\vartheta'). \tag{18}$$

We obtain

$$|\gamma|(\vartheta, z_\mathrm{d}, z_\mathrm{s}) = \kappa_0 \; g\left(\frac{\vartheta}{\theta_\mathrm{s}}\right), \tag{19}$$

with

$$g(x) = \frac{2}{x^2}\ln\frac{x}{2} - \frac{1}{x^2-1} + \frac{6x^2-4}{x^2(x^2-1)^{1.5}}\arctan\sqrt{\frac{x-1}{x+1}}, \tag{20}$$

for $x > 1$, and

$$g(x) = \frac{2}{x^2}\ln\frac{x}{2} - \frac{1}{x^2-1} + \frac{4-6x^2}{x^2(1-x^2)^{1.5}}\mathrm{arctanh}\sqrt{\frac{1-x}{x+1}}, \tag{21}$$

for $x < 1$. According to eq.(4) the tangential shear is

$$\gamma_\mathrm{t}(\vartheta) = \frac{m(\vartheta)}{\vartheta^2} - \kappa(\vartheta). \tag{22}$$

We assume a normalized source redshift distribution of the form

$$p_z(z) = \frac{\beta}{z_0^3 \; \Gamma\left(\frac{3}{\beta}\right)} \; z^2 \exp(-[z/z_0]^\beta), \tag{23}$$

(see Brainerd et al. 1996). The mean redshift of this distribution is proportional to z_0 and depends on the parameter β which describes how quickly the distribution falls off towards higher redshifts. We will use the values $\beta = 1.5$ and $z_0 = 1$. For these values the mean redshift $\langle z\rangle$ is given by $\langle z\rangle = 1.505 \; z_0$. With the distribution (23) we define a source distance-averaged surface density and shear

$$\kappa(\vartheta, z_\mathrm{d}) = \int dz_\mathrm{s} \; p_z(z_\mathrm{s}) \; \kappa(\vartheta, z_\mathrm{d}, z_\mathrm{s}), \tag{24}$$

$$\gamma_\mathrm{t}(\vartheta, z_\mathrm{d}) = \int dz_\mathrm{s} \; p_z(z_\mathrm{s}) \; \gamma_\mathrm{t}(\vartheta, z_\mathrm{d}, z_\mathrm{s}). \tag{25}$$

We emphasise here that the aperture mass M_ap in this form depends on three parameters: the lens mass M, the lens redshift z_d and the aperture radius θ. The mass and redshift dependence comes from the characteristic density δ_c, the scaling radius r_s and $D_\mathrm{d}, D_\mathrm{ds}$. Furthermore, M_ap depends on cosmology through the angular diameter distances, δ_c and r_s.

3 SIGNAL-TO-NOISE RATIO STATISTICS

S96 introduced a signal-to-noise ratio for the M_ap- statistics. An discretised estimator for (3) is given by

$$M_\mathrm{ap} = \frac{1}{n} \sum_i \; \epsilon_\mathrm{t}(\boldsymbol{\vartheta_i}) \; Q(|\boldsymbol{\vartheta_i}|), \tag{26}$$

where n is the number density of galaxy images and ϵ_t is the tangential component of the ellipticity of a galaxy at position $\boldsymbol{\vartheta_i}$, defined in analogy to (4). The dispersion σ_d of M_ap in the absence of lensing can be calculated by squaring (26) and taking the expectation value, which leads to

$$\sigma_\mathrm{d}^2 = \frac{\sigma_\epsilon^2}{2n^2} \; \sum_i Q^2(\vartheta_i), \tag{27}$$

where we used that the ellipticities of different images are not correlated and the dispersion of the observed ellipticity equals the intrinsic ellipticity distribution σ_ϵ. We take as reference values $\sigma_\epsilon = 0.2$ and $n = 30$ arcmin^{-2} (see S96). The expectation value of M_ap is

$$\langle M_\mathrm{ap}\rangle_\mathrm{d} = \frac{1}{n} \sum_i \; \gamma_\mathrm{t}(\vartheta_i) \; Q(\vartheta_i), \tag{28}$$

because the ellipticity is an unbiased estimate of the local shear in the case of weak lensing. Averaging (27) over the probability distribution for the spatial distribution of galaxies (see S96) one finds

$$\sigma_\mathrm{c}^2(\theta) = \frac{\pi\sigma_\epsilon^2}{n} \int_0^\theta d\vartheta \; \vartheta \; Q^2(\vartheta) = 0.2 \; \frac{\sigma_\epsilon^2}{n} \; \frac{1}{\theta^2}. \tag{29}$$

For reference, we rewrite (29) in useful units as

$$\sigma_\mathrm{c}(\theta) = 0.016\left(\frac{n}{30 \text{ arcmin}^{-2}}\right)^{-1/2}\left(\frac{\sigma_\epsilon}{0.2}\right)\left(\frac{\theta}{1 \text{ arcmin}}\right)^{-1}. \tag{30}$$

We define the signal-to-noise ratio as

$$S_\mathrm{c}(\theta) = \frac{M_\mathrm{ap}(\theta)}{\sigma_\mathrm{c}(\theta)}. \tag{31}$$

Note that σ_c depends only on the filter scale θ and the intrinsic properties of the source galaxies.

4 NUMBER OF HALOES

We assume dark matter haloes are distributed according to the Press-Schechter (1974) theory . In this formalism an analytical expression for the comoving number density of non-linear objects is derived on the basis of the spherical collapse theory assuming the initial density contrast to be a gaussian random field. The mass fraction in collapsed objects in the mass range dM about M is given by

$$f(M,z) \; dM = \sqrt{\frac{2}{\pi}} \; \frac{\delta_\mathrm{crit}(z)}{\sigma^2(M)} \; \left|\frac{d\sigma(M)}{dM}\right| \; \exp\left(-\frac{\delta_\mathrm{crit}^2(z)}{2\sigma^2(M)}\right) \; dM. \tag{32}$$

The redshift dependence of this function is given by the critical density treshold $\delta_\mathrm{crit}(z)$ for spherical collaps which depends on the linear growth factor $D_+(z)$ (Lacey & Cole 1993). $\sigma(M)$ is the present linear theory rms density fluctuation computed using a top hat filter and a CDM power spectrum (Bardeen et al. 1986) with shape parameter Γ and normalization σ_8. We use the fitting formulae given in NFW to compute $\sigma(M)$ and $\delta_\mathrm{crit}(z)$. If we multiply eq.(32) with $dV_\mathrm{p}(1+z)^3\bar\rho/M$,where $\bar\rho$ is the mean mass density today, we get the number of objects in the proper volume dV_p with mass in the intervall dM

$$N_\mathrm{halo}(M,z) \; dM \; dV_\mathrm{p} = (1+z)^3 \; \frac{\bar\rho}{M} \; f(M,z) \; dM \; dV_\mathrm{p}. \tag{33}$$

For fixed values of the lens redshift z_d and the aperture radius θ the aperture mass M_ap is a monotonically increasing function of the halo mass M (see Figure 1). This function can be inverted for a given value of M_ap. We write $M_\mathrm{t} = M_\mathrm{t}(M_\mathrm{ap}, z_\mathrm{d}, \theta)$ for the mass obtained by inversion. The number of haloes in a given proper volume with mass greater

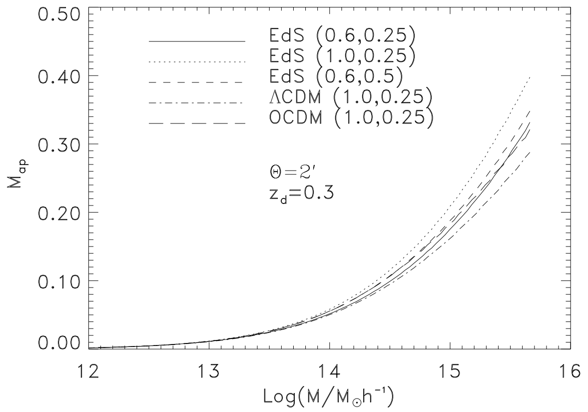

Figure 1. The aperture mass $M_{\rm ap}$, as defined in (1), computed for five different cosmologies as indicated by the line types. The numbers in parentheses are the normalization σ_8 and the shape parameter Γ. The lens redshift is $z_{\rm d} = 0.3$ and the aperture radius $\theta = 2$ arcmin.

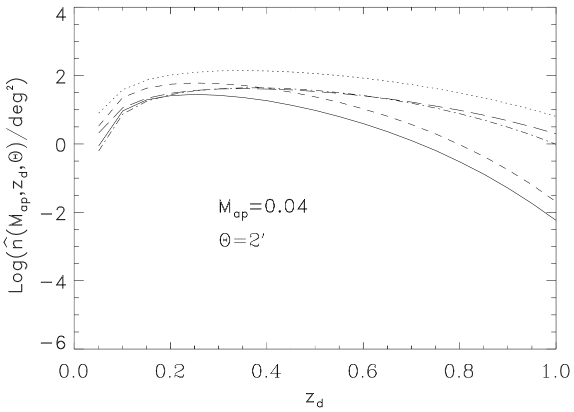

Figure 2. The number of haloes per square degree and unit redshift interval with aperture mass greater than 0.04, as defined in (40), as a function of lens redshift for the same cosmological models as indicated in Figure 1. The filter scale is $\theta = 2$ arcmin.

than $M_{\rm t}(M_{\rm ap}^0, z_{\rm d}, \theta)$, and thus an aperture mass larger than $M_{\rm ap}^0$, is given by

$$N(> M_{\rm ap}^0, \theta) = \int dV_{\rm p}\; G(z_{\rm d}, M_{\rm ap}^0, \theta), \tag{34}$$

with

$$G(z_{\rm d}, M_{\rm ap}^0, \theta) = \int dM\; N_{\rm halo}(M, z_{\rm d})\; H(M_{\rm ap}(M, z_{\rm d}, \theta) - M_{\rm ap}^0), \tag{35}$$

where $H(x-y)$ is the Heaviside step function. The integral is non-zero only for $M > M_{\rm t}$. Hence by introducing spherical polar coordinates

$$dV_{\rm p} = D_{\rm d}^2(z_{\rm d})\; dD_{\rm p}(z_{\rm d}), \quad dD_{\rm p}(z_{\rm d}) = \frac{dz_{\rm d}}{E(z_{\rm d})(1+z_{\rm d})}, \tag{36}$$

and

$$E(z_{\rm d}) = \sqrt{\Omega_{\rm d}(1+z_{\rm d})^3 + (1-\Omega_{\rm d}-\Omega_{\rm v})(1+z_{\rm d})^2 + \Omega_{\rm v}} \tag{37}$$

we obtain

$$N(> M_{\rm ap}, \theta) = \int dz_{\rm d}\; \frac{(1+z_{\rm d})^2}{E(z_{\rm d})}\; D_{\rm d}^2(z_{\rm d})\; \tilde{G}(z_{\rm d}, M_{\rm ap}, \theta), \tag{38}$$

with

$$\tilde{G}(z_{\rm d}, M_{\rm ap}, \theta) = \int_{M_{\rm t}(M_{\rm ap}, z_{\rm d}, \theta)}^{\infty} dM\; n(M, z_{\rm d}), \tag{39}$$

where $n(M, z_{\rm d}) = \frac{\bar{\rho}}{M}\, f(M, z_{\rm d})$. $N(> M_{\rm ap}, \theta)$ is the number of haloes per steradian with aperture mass larger than $M_{\rm ap}$. Since the aperture mass is determined by the tangential shear the number of haloes $N(> M_{\rm ap}, \theta)$ is an observable.

5 RESULTS

In this section we use the observable $N(> M_{\rm ap}, \theta)$ to constrain various cosmological models. We perform our calculations for the same five cosmological models as in Figure 1. For three of them, the power spectrum is approximately cluster normalized, which corresponds to $\sigma_8 \approx 0.6$ for an Einstein-de Sitter universe (EdS, $\Omega_{\rm d} = 1$, $\Omega_{\rm v} = 0$) and $\sigma_8 = 1$ for both an open universe (OCDM, $\Omega_{\rm d} = 0.3$, $\Omega_{\rm v} = 0$) and a spatially flat universe with cosmological constant (ΛCDM, $\Omega_{\rm d} = 0.3$, $\Omega_{\rm v} = 0.7$). For these models we use the shape parameter $\Gamma = 0.25$ which yields the best fit to the observed two-point correlation function of galaxies (Efstathiou 1996). The remaining two EdS models have higher normalization ($\sigma_8 = 1$, approximately corresponding to the COBE normalization) or a different shape parameter ($\Gamma = 0.5$).

In Figures 2 and 3 we plot the function

$$\hat{n}(M_{\rm ap}, z_{\rm d}, \theta) = \frac{(1+z_{\rm d})^2}{E(z_{\rm d})}\; D_{\rm d}^2(z_{\rm d})\; \tilde{G}(z_{\rm d}, M_{\rm ap}, \theta), \tag{40}$$

which is the number of haloes per unit solid angle and unit redshift interval with masses $M > M_{\rm t}(M_{\rm ap}, z_{\rm d}, \theta)$ for a filter scale of $\theta = 2'$ and the aperture masses $M_{\rm ap} = 0.04$ and $M_{\rm ap} = 0.08$ [see (39) for definition of $\tilde{G}(z_{\rm d}, M_{\rm ap}, \theta)$].

As expected from the evolution of the cluster mass function, the volume elements and the aperture mass $M_{\rm ap}$, we get different number densities of haloes for various cosmological parameters. We have a strong evolution with redshift in the $\Omega_{\rm d} = 1$ model and much less in the low-$\Omega_{\rm d}$ models. Furthermore, the number density of rich clusters at intermediate redshifts drops more rapidly in a critical density universe. The dependence of the volume elements and the aperture mass $M_{\rm ap}$ on the angular diameter distances enhances the difference between the cosmologies for high redshifts, and causes a decreasing number of haloes towards very small redshifts.

If we integrate (40) over lens redshift we obtain the observable $N(> M_{\rm ap}, \theta)$. We have plotted this observable in Figure 5 as a function of the aperture mass. The dependence of (38) on $M_{\rm ap}$ and θ can be understood as follows: Since the aperture mass $M_{\rm ap}$ is a monotonically increasing function of the halo mass (for a fixed redshift and filter scale; see Figure 1) we expect $N(> M_{\rm ap}, \theta)$ to decrease with increasing $M_{\rm ap}$. If we enlarge the filter radius the values of $M_{\rm ap}$ become

Table 1. The number of haloes per square degree with aperture mass greater than $M_{\rm ap} = 0.04$ and $M_{\rm ap} = 0.08$, as defined in (38), for the filter scale $\theta = 2$ arcmin. The redshift interval in brackets denote the integration range in (38). The number of haloes is computed for five cosmological models.

	EdS(0.6,0.25)	EdS(1,0.25)	EdS(0.6,0.5)	OCDM(1,0.25)	ΛCDM(1,0.25)
$N(>0.04, 2')$ $z_{\rm d} \in [0,1]$	9.42	71.66	21.66	21.44	20.92
$N(>0.08, 2')$ $z_{\rm d} \in [0,1]$	0.47	13.00	1.23	2.46	1.74
$N(>0.04, 2')$ $z_{\rm d} \in [0.15, 0.4]$	6.18	30.66	13.54	9.07	9.02
$N(>0.04, 2')$ $z_{\rm d} \in [0.4, 1]$	2.34	37.09	5.89	11.23	11.14
$N(>0.08, 2')$ $z_{\rm d} \in [0.15, 0.4]$	0.36	6.94	0.93	1.37	0.99
$N(>0.08, 2')$ $z_{\rm d} \in [0.4, 1]$	0.06	5.29	0.17	0.97	0.71

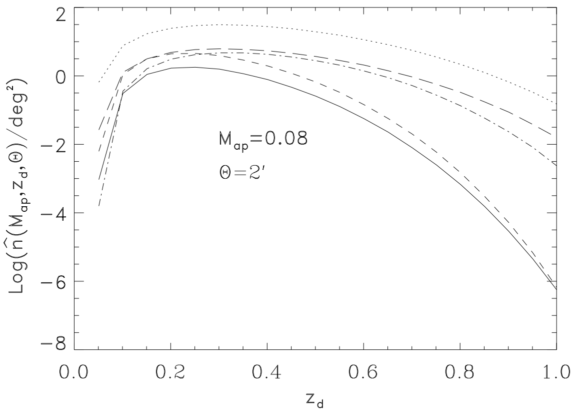

Figure 3. Same as Fig. 2, for $M_{\rm ap} = 0.08$. The aperture mass is a monotonically increasing function of the halo mass (see Figure 1). Furthermore, rich clusters evolve more than clusters with low mass. Therefore, compared to Figure 2, the number density of haloes is smaller and we observe a stronger evolution in the various cosmologies.

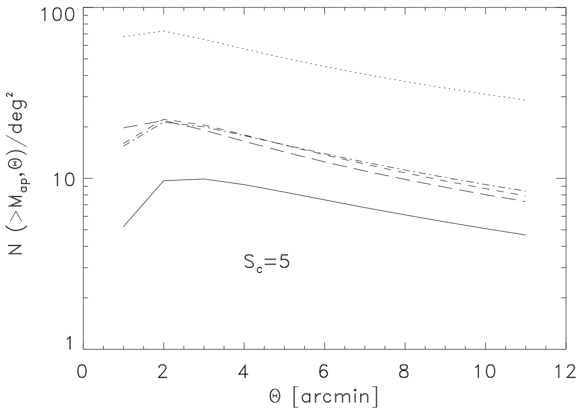

Figure 4. The number of haloes per square degree with aperture mass greater than $M_{\rm ap} = 5\,\sigma_{\rm c}(\theta)$, as defined in (38), as a function of the filter scale for the same cosmological models as indicated in Figure 1. For $\theta = 2'$ we obtain a maximum number of haloes for all cosmologies at a fixed signal-to-noise ratio $S_{\rm c} = 5$.

smaller and, because of the monotony of $M_{\rm ap}$ in the halo mass, for fixed $M_{\rm ap}$ the corresponding threshold mass $M_{\rm t}$ increases. Therefore the number of haloes decreases with increasing filter size. Because of this behaviour of $N(>M_{\rm ap}, \theta)$ we can select a filter radius and a value for $M_{\rm ap}$ which allows us to count a sufficient number of haloes used for finding a significant difference between the various cosmologies. In practice we have to determine a signal-to-noise ratio threshold above which we can consider a significant detection. We will use here mainly a threshold value of $S_{\rm c} = 5$.

In Figure 4 we have plotted the number of haloes per square degree with aperture masses yielding a signal-to-noise ratio above the threshold value $S_{\rm c} = 5$ for different filter scales. According to Figure 4 we count in all cosmologies the maximum number of haloes for $\theta = 2$ arcmin. We will use this 'optimal' filter scale for our calculations. According to (31) the corresponding aperture mass is $M_{\rm ap} = 0.04$ for the 'optimal' filter radius and the signal-to-noise ratio threshold.

In real observations, the derived value of $M_{\rm ap}$ will differ from the true one due to several effects. First, the intrinsic ellipticity distribution of the source galaxies causes noise in the measurement of $M_{\rm ap}$ which is given by (29). Second, the number of source galaxies in the filter will have at least Poissonian noise. And third, halos are not isolated, but there will be perturbing mass inhomogeneities along the line-of-sight to the halo. Comparing the first two sources of errors, the first dominates (see Schneider et al. (1998)), and so we con-

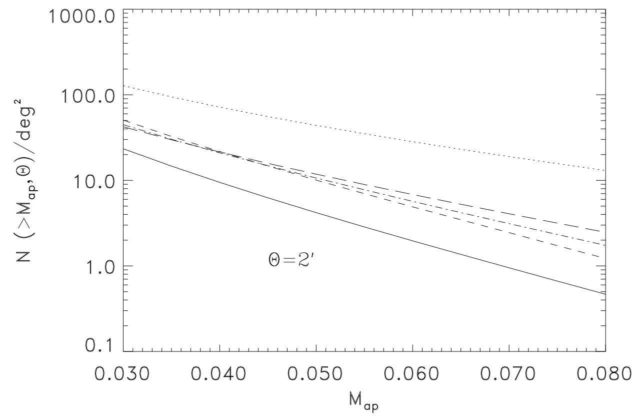

Figure 5. The number of haloes per square degree with aperture mass greater than $M_{\rm ap}$, as defined in (38), as a function of $M_{\rm ap}$ for the same cosmological models as indicated in Figure 1. The filter scale is $\theta = 2$ arcmin.

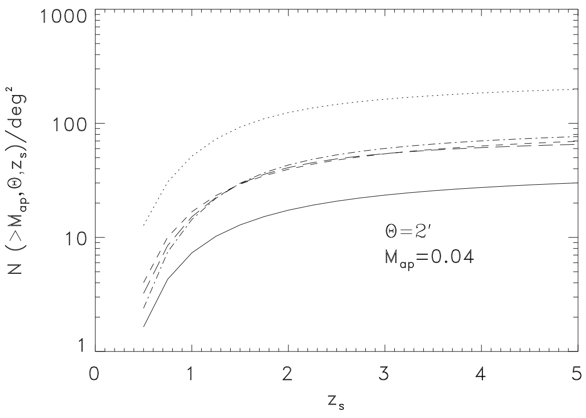

Figure 7. The number of haloes per square degree with aperture mass greater than $M_{\rm ap} = 0.04$, as defined in (38), as a function of source redshift for the same cosmological models as indicated in Figure 1. All sources are assumed to be at the same redshift. The filter scale is $\theta = 2$ arcmin.

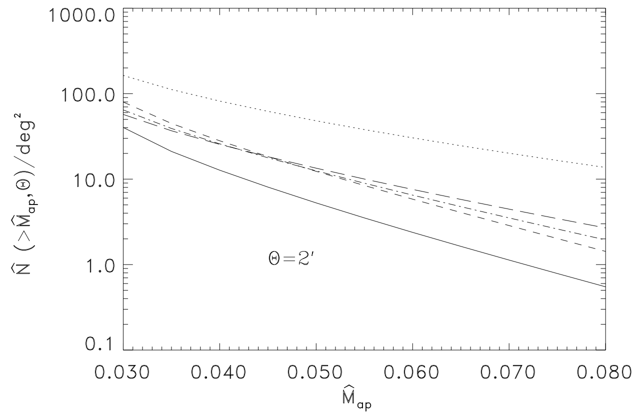

Figure 6. The convolution of the number of haloes per square degree with aperture mass greater than $M_{\rm ap}$ with the distribution (41), as defined in (42), as a function of $M_{\rm ap}$ for the same cosmological models as indicated in Figure 1. The filter scale is $\theta = 2$ arcmin. Compared to Figure 5 the number of haloes is shifted to higher values.

sider $\sigma_{\rm c}$ as the uncertainty with which we can measure $M_{\rm ap}$. The third source of error cannot be modelled analytically, but must be estimated through ray-tracing simulations such as those carried out by Jain, Seljak & White (1998). Then, by taking into account only the noise coming from the intrinsic ellipticity distribution of the source galaxies, we assume that the deviation $\Delta M_{\rm ap}$ between the true value of $M_{\rm ap}$ and the measured one $\hat{M}_{\rm ap}$ is Gaussian,

$$p(\Delta M_{\rm ap},\theta) = \frac{1}{\sqrt{2\pi}\ \sigma_{\rm c}(\theta)} \exp\left(-\frac{\Delta M_{\rm ap}^2}{2\ \sigma_{\rm c}^2(\theta)}\right). \tag{41}$$

In Figure 6 we have plotted the convolution $\hat{N}(>\hat{M}_{\rm ap},\theta)$ of $N(>M_{\rm ap},\theta)$ with the distribution (41) for the filter scale $\theta = 2'$,

$$\hat{N}(>\hat{M}_{\rm ap},\theta) = \int dM_{\rm ap}\ N(>M_{\rm ap},\theta)\ p(\hat{M}_{\rm ap} - M_{\rm ap},\theta). \tag{42}$$

In comparison with the non-convolved function (see Figure 5) the values of (42) are only slightly enhanced for the values of $M_{\rm ap}$ we are interested in (e.g., $M_{\rm ap} = 0.04, 0.08$). Therefore, in the following discussion we shall neglect the difference between the distributions of $M_{\rm ap}$ and $\hat{M}_{\rm ap}$.

We shall now discuss whether from measuring the number density of haloes above a given threshold $M_{\rm ap}$, one can distinguish between the various cosmological models mentioned at the beginning of this section. From Figs. 5 and 6, we see that the EdS models with $\sigma_8 = 0.6$ and $\Gamma = 0.25$ [hereafter EdS(0.6,0.25)], and with $\sigma_8 = 1$ and $\Gamma = 0.25$ [hereafter EdS(1,0.25)], have a considerably lower and higher, respectively, number density of haloes for given $M_{\rm ap}$ than the three other models. From the numbers in Table 1, considering a value of $M_{\rm ap} = 0.04$ or signal-to-noise of 5, it is clear that these two cosmologies can be distinguished significantly (by which we mean that the Poisson error bars do not overlap) from the other three already with 1 $\deg^2$ of a deep imaging survey. To distinguish between the other three cosmologies [EdS(0.6,0.5), OCDM, ΛCDM], a larger-area survey is needed. Taking the projected MEGACAM survey with its expected 25 $\deg^2$ as an example (Mellier et al. 1998), one sees from the numbers in Table 1 that at $M_{\rm ap} = 0.08$ (signal-to-noise of 10), this survey is more than sufficient to allow a clear distinction of these three cosmologies. We therefore conclude that the currently planned wide-field imaging surveys will allow to separate between the most popular currently discussed cosmological models.

In order to get a more precise handle on the values of the cosmological parameters and/or the shape of the initial power spectrum, more detailed information may be used. Assuming that the haloes giving rise to measurements of $M_{\rm ap}$ are not completely dark, but cluster-like (though possibly with a broad range of mass-to-light ratios), one might be able to identify a measured halo with a galaxy overdensity on the sky and/or in redshift, and thus determine the redshift of the corresponding halo, using either photometric redshift techniques or spectroscopy. In this case, the redshift dependence of the halo distribution can be measured. As shown in Figs. 2 and 3, the redshift evolution of the halo density as probed by $M_{\rm ap}$ is quite different in the cosmologies considered here.

In Table 1 we have also displayed the number of haloes per square degree with aperture mass greater than $M_{\rm ap} = 0.04$ and $M_{\rm ap} = 0.08$ for the filter scale $\theta = 2'$ for the five cosmological models, using two different redshift intervals, $z \in [0.15, 0.4]$ and $z \in [0.4, 1]$. By comparing the halo densities in the different redshift intervals for the various cosmologies in Figs. 2 and 3, we expect the largest differences between the cosmological models for $M_{\rm ap} = 0.08$. The reason for this is the stronger evolution for the rich cluster mass function which corresponds to large values of the aperture mass (see Figure 1). Whereas the EdS(0.6,0.25) and EdS(1,0.25) models are again very different from the other three, the use of redshift information greatly helps to distinguish the EdS(0.6,0.5) model from the two low-density models. For the latter, a survey area of less than 3 deg^2 would be sufficient.

One might think of another way to obtain redshift information, namely to use source galaxies at different redshifts (distinguished, say, by photometric redshift estimates). To investigate this effect, we have plotted in Figure 7 the dependence of the number of haloes on the redshift of the sources for $M_{\rm ap} = 0.04$ and $\theta = 2'$. All sources are assumed to be at the same redshift $z_{\rm s}$. Whereas the number density of haloes as measured with $M_{\rm ap}$ depends strongly on the source redshift, this dependence is quite similar in all cosmologies, except at rather low redshifts, $z_{\rm s} \sim 0.6$. However, their number density is likely to be fairly small, so that the differences seen in Fig. 7 will be very difficult to measure. We therefore discard this indicator at this point.

6 DISCUSSION AND CONCLUSIONS

In this paper we investigated the statistics of high signal-to-noise peaks in the aperture mass map in various cosmological models. We constructed the observable number of peaks in the aperture mass $N(> M_{\rm ap}, \theta)$ using the Press-Schechter theory for evaluating the number density of haloes and the universal density profile of NFW. The observable number density of high signal-to-noise peaks in the aperture mass map – or in other words, the number density of mass-selected haloes – is large in all cosmological models considered here, and range from ~ 10 deg^{-2} for a cluster normalized EdS model to ~ 70 deg^{-2} for a COBE-normalized EdS model, quoted for a signal-to-noise ratio of 5. Even for a signal-to-noise ratio of 10, the number density of detectable haloes is about one per square degree. Hence, in future wide-field imaging surveys, such haloes will easily be found, so that a mass-selected sample of 'clusters' is within reach. Given that the cluster abundance has been used extensively as a cosmological probe, this mass-selected sample will be extremely useful to related observations to theoretical predictions.

We estimated that a few square degrees of a deep wide-field imaging survey will be sufficient to distinguish between some of the most popular cosmological parameter sets. In particular, cluster-normalized low-density universes can be easily distinguished from a cluster-normalized EdS model, which is mainly due to the fact that in the latter, the number density of haloes at a redshift of $z_{\rm d} \sim 0.3$, which is mainly probed by our technique, is predicted to be considerably lower than in the open models.

Whereas our estimates on the number density of detectable haloes are based on several simplifying assumptions (e.g., that halo number density can be obtained from the Press-Schechter theory, that the mass density is spherical and follows an NFW profile, that halos are isolated, etc.) and therefore probably not very accurate, the numbers obtained should approximately reflect the true situation. In particular, the relative abundance as a function of $M_{\rm ap}$ and in dependence on cosmological parameters will be the same as calculated here. For more quantitative estimates, ray-tracing calculations in a model universe obtained from N-body simulations have to be used. With results obtained from there, more sensitive statistics for the determination of cosmological parameters can be derived.

ACKNOWLEDGMENTS

We want to thank C.S. Frenk for providing us the routine for computing the NFW profile parameter. This work was supported by the "Sonderforschungsbereich 375-95 für Astro-Teilchenphysik" der Deutschen Forschungsgemeinschaft.

REFERENCES

Bardeen, J.M., Bond, J.R., Kaiser, N. & Szalay, A.S. 1986, ApJ 304, 15
Bartelmann, M. 1996, A&A 313, 697
Bartelmann, M., Huss, A., Colberg, J.M., Jenkins, A. & Pearce, F.R. 1998, A&A 330, 1
Borgani, S., Rosati, P., Tozzi, P. & Norman, C. 1998, preprint
Brainerd, T.G., Blandford, R.D. & Smail, I. 1996, ApJ 466, 623
Efstathiou, G. 1996, in: *Cosmology and large scale structure*, Les Houches Session LX, R. Scheffer, J. Silk, M. Spiro & J. Zinn-Justin (eds.), North-Holland, p.133.
Eke, V.R., Cole, S. & Frenk, C.S. 1996, MNRAS 282, 263
Fort, B., Prieur, J.L., Mathez, G., Mellier, Y. & Soucail,G. 1988, A&A 200, L17
Fort, B. & Mellier, Y. 1994, A&AR5, 239
Jain, B., Seljak, U. & White, S.D.M. 1998, astro-ph/ 9804238
Kaiser, N. & Squires, G. 1993, ApJ 404, 441
Kaiser, N., Squires, G., Fahlman, G. & Woods, D. 1994, astro-ph/9407004
Kaiser, N. 1995, ApJ 1995, L1
Lacey, C. & Cole, S. 1993, MNRAS 262, 627
Luppino, G.A. & Kaiser, N. 1997, ApJ 475, 20
Mellier, Y., van Waerbeke, L. & Bernardeau, F. 1998, preprint
Navarro, J.F, Frenk, C.S. & White, S.D.M. 1996, ApJ 462, 563
Navarro, J.F, Frenk, C.S. & White, S.D.M. 1997, ApJ 490, 493
Press, W.H. & Schechter, P. 1974, ApJ 187, 425
Schneider, P. 1996, MNRAS 283, 837
Schneider, P., van Waerbeke, L., Jain, B. & Kruse, G. 1998, MNRAS 296, 873
Seitz, S., Saglia, R.P., Bender, R., Hopp, U., Belloni, P. & Ziegler, B., astro-ph/9706023
Soucail, G., Fort, B., Mellier, Y. & Picat, J.P. 1987, A&A 184, L14
Squires, G. & Kaiser, N. 1996, ApJ 473, 65
Tyson, J.A., Valdes, F. & Wenk, R.A. 1990, ApJ 349, L1

Webster, R.L. 1985, MNRAS 213, 871
White, S.D.M., Efstathiou, G. & Frenk, C.S. 1993, MNRAS 262, 1023
Yee, H.K.C., Ellingson, E., Bechtold, J., Carlberg, R.G. & Cuillandre, J.-C. 1996, AJ 111, 1783

This paper has been produced using the Royal Astronomical Society/Blackwell Science LaTeX style file.